

# STUDY ON EVALUATION OF WALL THINNING IN A STRUCTURAL MEMBER USING LAMB WAVES: MODE SEPARATION USING THE MARS METHOD

Masanori Takuma,<sup>1\*</sup> Ken-ichi Saitoh,<sup>1</sup> Yoshimasa Takahashi<sup>1</sup>, and Tomohiro Sato<sup>1</sup>

(Received June 7, 2022; accepted December 5, 2022)

## Abstract

The nondestructive ultrasonic wave inspection method is widely used for the inspection of a variety of structures. However, significant time and labor are required for ultrasonic wave inspection as its attenuation must be carefully monitored. Against this background, Lamb waves, in which long-distance propagation is possible, have attracted attention. Analysis is difficult, however, because Lamb wave speed dispersibility is large and plural single mode waves pile on. To address this problem, the movable auto regressive system (MARS) method is applied to separate each single mode. Specifically, waves were separated into single mode waves, and the process for evaluating the thinning state is proposed. The effectiveness of this process was demonstrated by the evaluation results.

**Key words:** Damage evaluation, Nondestructive inspection, Ultrasonic, Lamb wave, Movable auto regressive system, Wall thinning

## 1 Introduction

In order to prevent trouble and disruptive accidents related to equipment and structures, the ultrasonic flaw detection method is regularly employed to inspect defects and damage. However, in order to determine and evaluate the shapes, dimensions, and position of defects, it is necessary to consider the flaw detection of the entire inspection surface and the attenuation of ultrasonic waves. As such, inspection requires considerable time and labor. Against this background, Lamb waves that can be propagated over long distances in thin plates and thin-walled circular tubes are attracting attention, and their application is being attempted to large structures such as pipelines.<sup>1)</sup> Since the propagation characteristics (i.e., phase velocity and group velocity) of Lamb waves include velocity dispersibility that varies greatly depending on the material, plate thickness, and frequency, the superposition in the propagation process of multiple mode waves with different sound velocities complicates waveforms and makes analyses difficult. These problems hinder the widespread adoption of Lamb waves. Therefore, in inspections adopting Lamb waves, the received waveform is analyzed separately for each mode, but in many cases, inspections in which a single mode with low frequency is excited are being carried out.<sup>2)-7)</sup> In order to solve the problem of the trade-off relationship between

---

<sup>1</sup> Department of Mechanical Engineering, Kansai University, Suita, Osaka 564-8680, Japan

\* Correspondence to: Masanori Takuma, Department of Mechanical Engineering, Kansai University, Suita, Osaka 564-8680. E-mail: t940081@kansai-u.ac.jp

frequency and defect detection resolution, it is necessary to separate the waveform in the high-frequency range where multiple modes overlap into a single mode waveform.

In this study, in order to improve the detection accuracy of defects using Lamb waves with high-frequency components, a dynamic frequency analysis, namely, the movable auto regressive system (MARS) method<sup>8)</sup> was applied to the separation of waves in which multiple modes were superimposed. Then, the evaluation results for the thinning state (i.e., the depth and width of the thinning part) of the member (e.g., plate) based on the characteristics of each mode wave after separation are reported.

## 2 Specimen, Experimental and Analysis Method

### 2.1 Specimen and experimental method

Figure 1 shows the shape and dimensions of the specimen and the schematic diagram of the experimental and the measuring equipment. A stainless steel plate (SUS304) used for structures such as chemical plants was employed for the specimen, and its thickness was set to 2 mm, which easily generates Lamb waves. The other dimensions were determined in order to not be affected by the reflected waves from the edges of the plate. Specimens with six types of grooves (see Fig. 1) that simulated wall thinning by corrosion on the back surface were prepared.

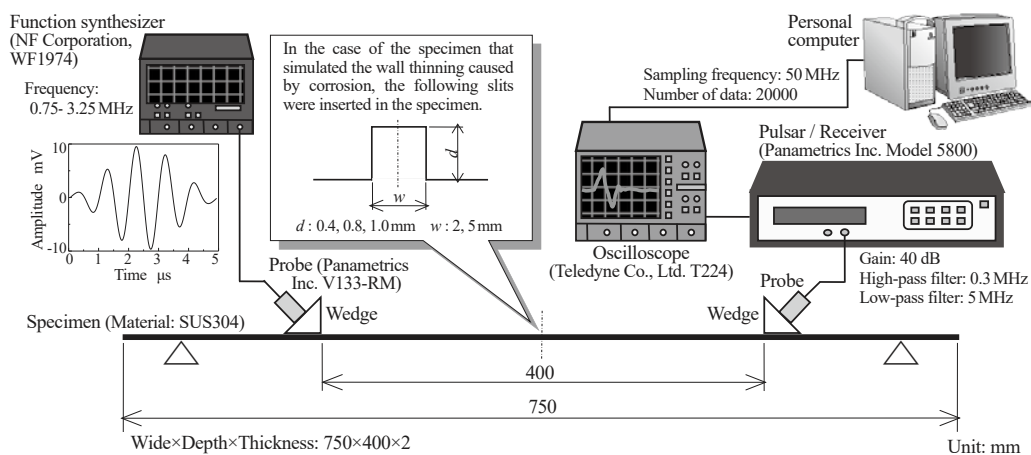


**Fig.1** Conception diagram of specimen, experimental and measurement equipment. In this study, several kinds of specimens have been prepared. One has the uniform thickness, and the others have the slits simulated the wall thinning by corrosion.

The experimental and the measuring equipment consists of a function synthesizer, pulse transmitter/receiver, oscilloscope, ultrasonic probe, variable angle wedge (variable angle: 0–60 deg) that excites Lamb waves, and a personal computer. The positions of the wedges and probes are shown in Fig. 1; glycerin paste was applied between both and they were crimped. Considering the analysis time for evaluating the thinning state (i.e., groove depth and width), the frequency and angle in which the two modes are excited were adopted. Here, the excitation angle  $\theta$  was derived from Snell's law ( $\sin \theta = c_w / c$ ), which consists of the velocity  $c$  to the frequency  $f$  in the dispersion curve of the phase velocity and the longitudinal wave sound velocity  $c_w$  of the wedge.

Figure 2 shows the occurrence states of each mode at frequency  $f$  and incident angle  $\theta$ . In the angle range (i.e., 20–50 deg) of the wedge and the frequency range (i.e., 0.75–3.25 MHz), the Lamb waves of S1 and A1 modes were excited, and these modes were employed. Using the personal computer shown in Fig. 1, the averaging process was performed on the number of 1,000 waves detected at each individual frequency and angle.

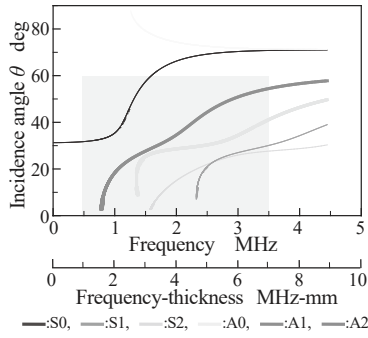


**Fig.2** Relationship between frequency (or frequency-thickness) and incidence angle. The settable range in this study is shown by gray color. From that result, it is clear that the others except S0 and A0 mode are suitable for analysis.

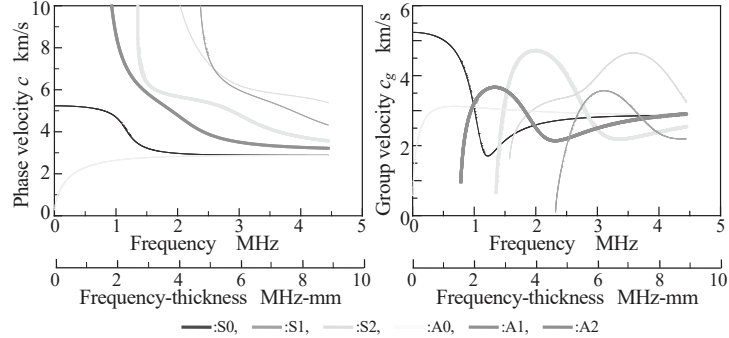


**Fig.3** Dispersion curve of phase and group velocity. Each mode speed approaches the surface wave speed which is about 0.9 times of transversal wave speed, when the frequency (or frequency-thickness) grows big. The validity of the solution method of the equation of Rayleigh-Lamb in this study was confirmed by comparing those results of aluminum reported in the previous study.

## 2.2 Experimental and analysis method

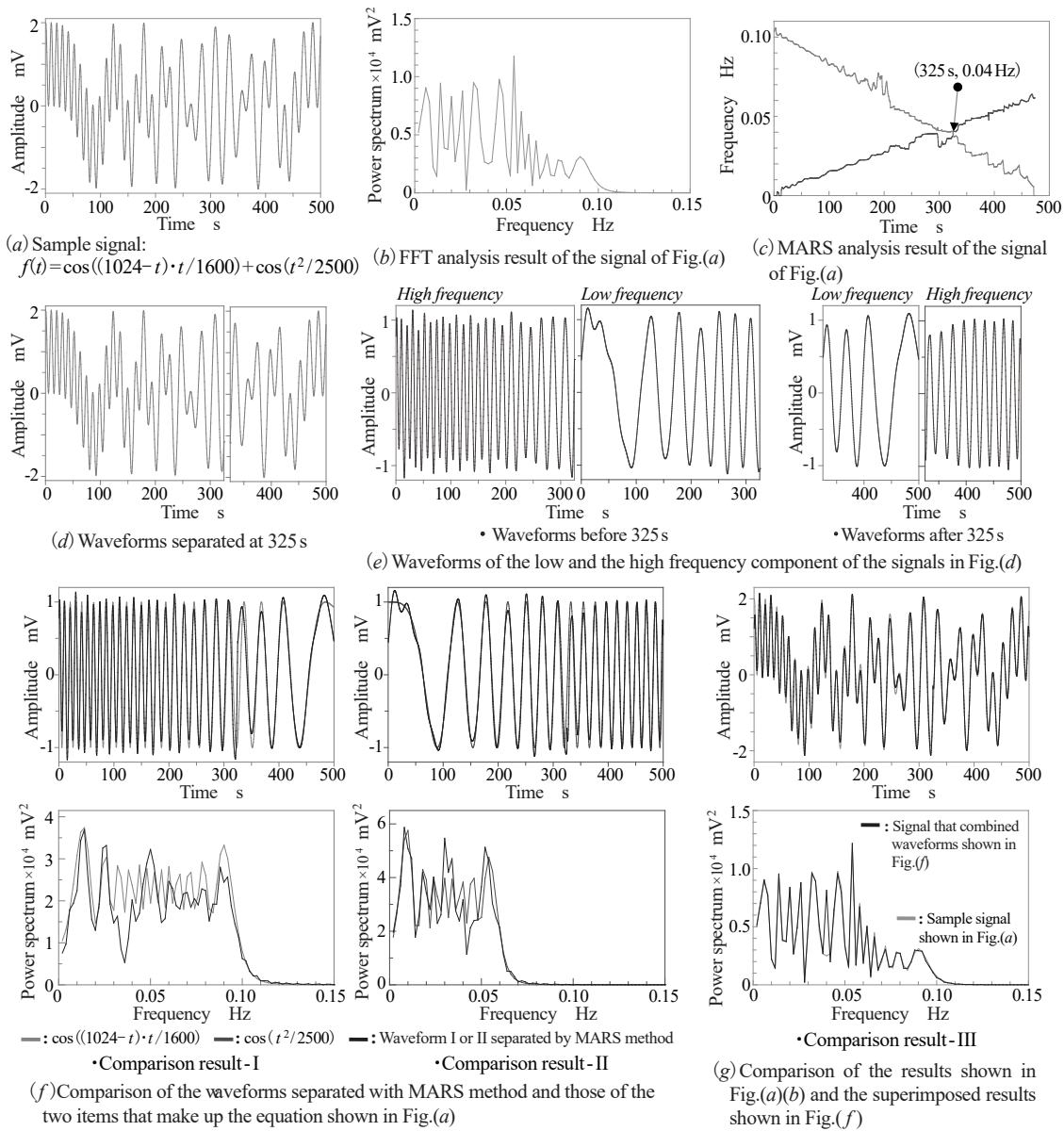
Figure 3 shows the results that solved the equation of Rayleigh and Lamb, and the velocity dispersion curves of phase velocity  $c$  and group velocity  $c_g$  in A0 to A2 mode and S0 to S2 mode. The thick line in the figure shows the S1 and A1 modes used in this study. In order to separate the Lamb waves on which the multiple modes are superimposed, the MARS method, which separates the waves based on their frequency changes, was applied.

Figure 4 shows an example of the mode separation of a sample signal (see Fig. 4(a)) in which two waveforms with velocity dispersibility were superimposed.

(1) Figure 4 (b) (c) show the results of the frequency analysis and the analysis with the MARS method of the signal shown in Fig. 4(a). These results confirm that the frequency band of that signal is 0 to 0.1 Hz and that there are two modes (i.e., red and blue color lines in the figure) with different velocity dispersibility and a cross point (i.e., time: 325 s, frequency: 0.04 Hz) between them.

(2) The signal shown in Fig. 4(a) is divided into the two waveforms shown in Fig. 4(d) at 325 s. They are then separated into the four waveforms shown in Fig. 4(e) by the high- and low-pass filtering of 0.04 Hz.

(3) The two black color waveforms shown in Fig. 4(f) are derived by the following two processes. The first is the process for connecting the waveforms of the high-frequency



**Fig.4** An example of analysis results with MARS method. The results from Fig.(a) to Fig.(f) show the separation process of a signal consisting of the two terms in the right side of function  $f(t)$  shown in Fig.(a) with MARS method. In Fig.(f), it is clear that the two kinds of the cosine waveforms in that function  $f(t)$  and their FFT analysis results are similar to the two types of the waveforms after separation and their FFT analysis results. Therefore, it is clear that the waveform separation with MARS method is suitable. Also, Fig.(g) shows the comparison of a sample signal shown in Fig.(a) and the combined signal of the two separated waveforms. From this result, it is clear that the application of this method is effective.

component in the first half and the low-frequency component in the second half of 325 s. The second is the process for connecting the waveforms of the low-frequency component in the first half and the high-frequency component in the second half of 325 s.

The two waveforms separated in this way and their frequency distributions are compared

with the first term (red color) and the second term (blue color) on the right side of the function  $f(t)$  representing the signal shown in Fig. 4(a). The comparison results verify the validity of the mode separation by the MARS method. Figure 4(f) shows the results, which clarify the following:

(I) The amplitude values are almost the same.

(II) Based on the characteristics of the waveform that changes with the passage of time, it became clear that the red color waveform changes to the low frequency and the blue color waveform changes to the high frequency. These tendencies are consistent with the frequency changes (see Fig. (c)) in the first and the second term on the right side of the function  $f(t)$ .

(III) Large differences are not observed in the start point, the end point, and the phase of the waveforms.

(IV) From the results of FFT analysis, it is clear that the frequency distributions of each term of the function  $f(t)$  and the separated signals are similar.

A wave is composed of amplitude, frequency, and phase, and each separate waveform and that of function  $f(t)$  exhibits the same tendency for these three points. As such, the separation with the MARS method is considered appropriate. In contrast, Fig. 4(g) shows the signal obtained by adding two waveforms (i.e., the black color line shown in Fig. 4(f)) after separation and the result of that frequency analysis. Comparing these results and the waveform and the frequency distribution shown in Fig. 4(a) (b), the amplitudes and the frequency distributions that fluctuate with time are almost the same, indicating that the separation with this method is appropriate. Similar results were obtained with the sample signals superposed with other periodic functions in which the frequency changes over time.

### 3 Experimental results and discussion

#### 3.1 Excitation and mode separation of Lamb wave

Figure 5 shows the results in which both S1 and A1 modes are excited. The conditions of the frequency and incident angle of the ultrasonic wave with reference to the velocity dispersion curve shown in Fig. 3 are 3 MHz and 34.4 deg, respectively. Figure 5(a) shows the detected Lamb wave and the result of superimposing the dispersion curve of the group velocity  $c_g$  on its STFT result. The display format of the dispersion curve, which has the group velocity on the vertical axis and the frequency on the horizontal axis, has been converted to the STFT display format, which has the frequency on the vertical axis and the time on the horizontal axis. Based on these results, mode separation with the MARS method was attempted, because the excitation of both S1 and A1 modes was confirmed. The results are shown in Fig. 5(b). The frequency components of both modes changed with the passage of time, and the existence of a cross point (time: 189.78  $\mu$ s, frequency: 3.22 MHz) was confirmed. Therefore, as shown in Fig. 5(c), the waveform was divided into two at 189.78  $\mu$ s, and these waveforms were processed by band-pass filter I from 0.3 to 3.22 MHz and filter II from 3.22 to 4 MHz. These results are shown in Fig. 5(d). The top part of Fig. 5(e) shows the results of connecting the waveforms. One of the two waveforms is the combination of the waveform with 0.3 to 3.22 MHz in 50 to 189.78  $\mu$ s and that with 3.22 to 4 MHz in 189.78 to 450  $\mu$ s. The other is the combination of the waveform with 3.22 to 4 MHz in 50 to 189.78  $\mu$ s and that with 0.3 to 3.22 MHz in 189.78 to 450  $\mu$ s. The bottom part of that figure is the result of

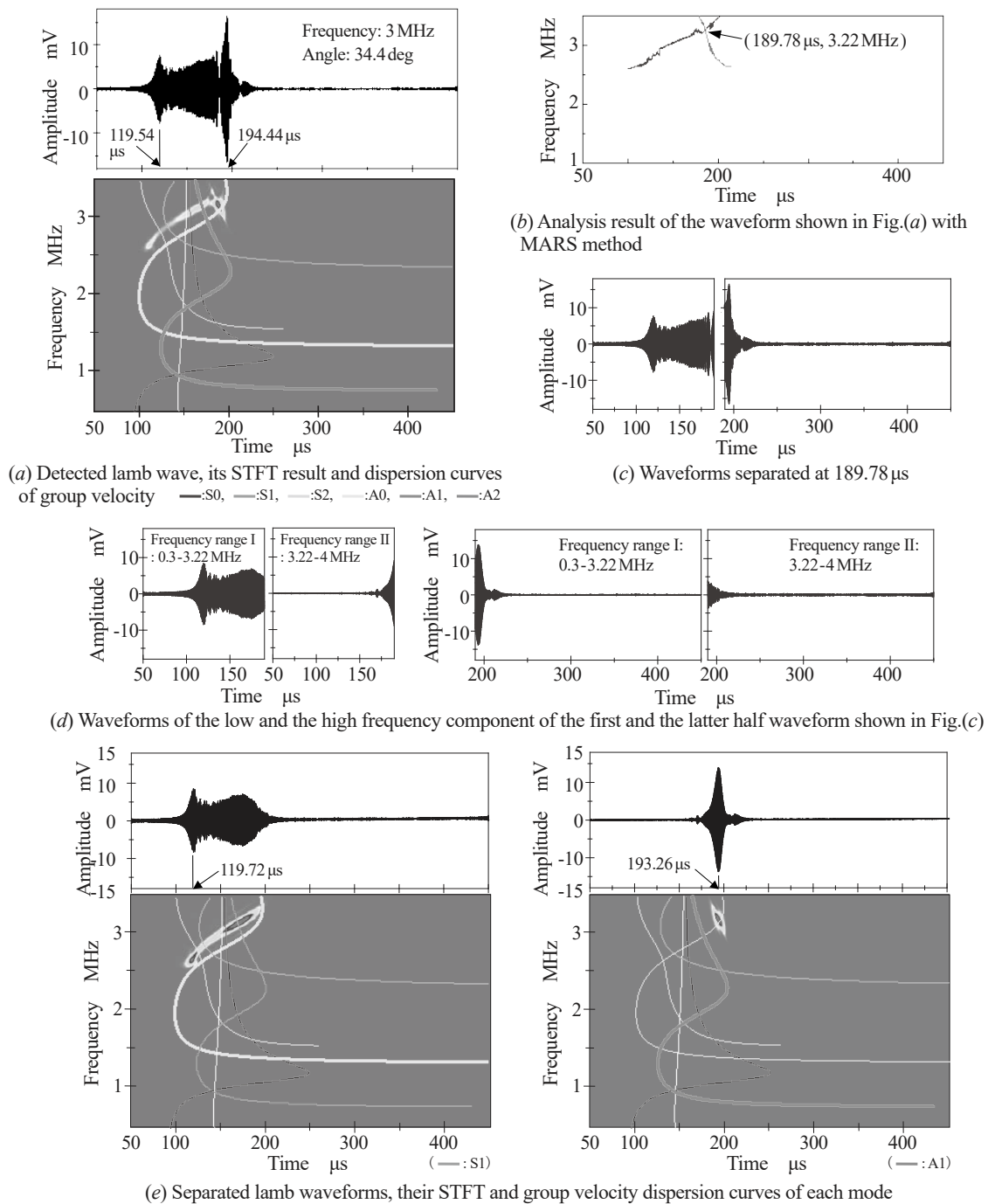


**Fig.5** Example of the result of separating a lamb wave in which two modes are intermingled into each single mode with MARS method. Figure (b) to Fig.(d) show the process of separating the lamb wave shown in Fig.(a) (cf. flow of Fig.4). From the results of Fig.(e), it was found that S1 and A1 mode wave are on the left and right, respectively. Therefore, by using MARS method, it was clarified that the lamb waves consisting of multiple modes were able to be separated into individual single mode wave.

superimposing the STFT results of those waveforms and the dispersion curve of group velocity. As a result of identifying the mode of each waveform from these data, it is evident that the top left waveform in Fig. 5(e) is S1 mode and the top right waveform in the same figure is A1 mode. By comparing the waveforms before (i.e., Fig. 5(a)) and after separation (i.e., Fig. 5(e)), the following became clear. The time when the amplitude of the waveform of S1 mode shows the maximum value is almost the same as that before the separation. This result was also observed in the waveform of A1 mode. Also, the waveform distortion is not observed. It is believed that the mode separation is performed properly, because the same tendencies were observed for the Lamb waves excited under other conditions.

### 3.2 Evaluation of the groove shape that simulated the corrosion defect

The results of evaluating the thinning state from the characteristics of the waveform of each mode after separation are described. The MARS method is applied to the Lamb waves detected from the specimen with a thickness of 2 mm and the grooved specimens (see Fig. 1) that simulated the corrosion thinning, and mode separation is performed. Next, the wall thinning (i.e., groove depth) and width (i.e., groove width) were evaluated from the characteristics of the waveforms of each mode detected from both specimens. Here, because the Lamb wave shown in Fig. 5 detected from the specimen with a thickness of 2 mm is used, the excitation conditions of the wave for the grooved specimens are the same as that in Fig. 5. In short, the frequency  $f$  is 3.0 MHz and the incident angle  $\theta$  is 34.4 deg.

As a result of examining the influences of groove depth and width to Lamb waves from velocity dispersion curves, it was found that the changes in the velocity by the depth (i.e., thickness) and the distance by the width cause the difference in propagation time. Here, although it cannot be said that this is sufficient as an evaluation method of the thinning state, it is assumed that the mode conversion does not occur in that part (i.e., groove part). Therefore, the passage time  $T$  of that part has the following relationship between the groove depth  $d_i$  and width  $w_j$ . Also, the  $c_{Di}$  is the group velocity of the Lamb wave at the thickness of  $D_i$  (= plate thickness  $D_0$  - groove depth  $d_i$ ).

$$w_j / c_{Di} = T \quad (1)$$

Here, if the time required for the propagation distance of  $w_j$  in the specimen with the thickness of  $D_0$  is  $T_h$  and there is no defect that affects the arrival time of that wave, the arrival time difference  $\Delta T_{ij}$  generated by the propagation of the groove part is derived from the following equation.

$$(w_j / c_{Di}) - (w_j / c_0) = T - T_h = \Delta T_{ij} \quad (2)$$

By expressing the above equation with the groove width  $w_j$ , it becomes the relational expression with the group velocity  $c_{Di}$ .

$$w_j = ((c_{Di} \times c_0) / (c_0 - c_{Di})) \times \Delta T_{ij} \quad (3)$$

The above expression is derived for each mode wave separated from the Lamb wave propagating through the groove part. In this report, the thinning state is evaluated by solving the simultaneous linear equations of Eq. (3) obtained from the two mode waves. The results are described below.

Figure 6 shows the detected Lamb waves and their analysis results from the grooved specimen type I (depth: 0.4 mm, width: 5.0 mm) and type II (depth: 1.0 mm, width: 2.0 mm) under the same excitation conditions as in Fig. 5. In the top, middle, and bottom part of the

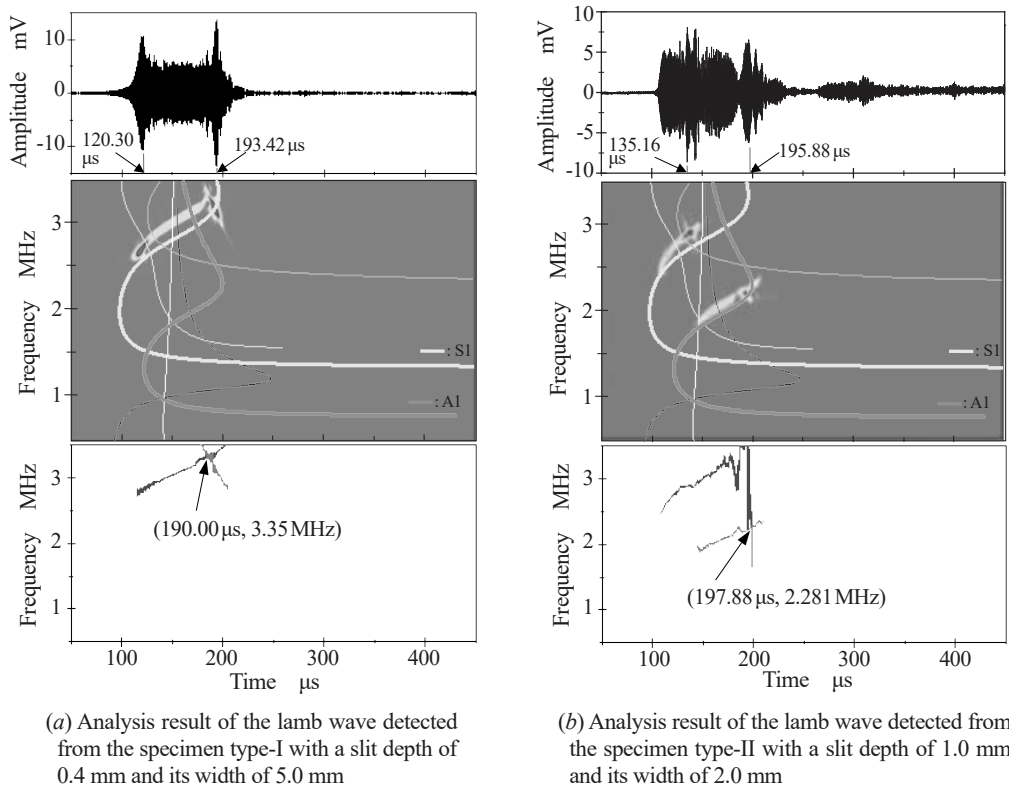
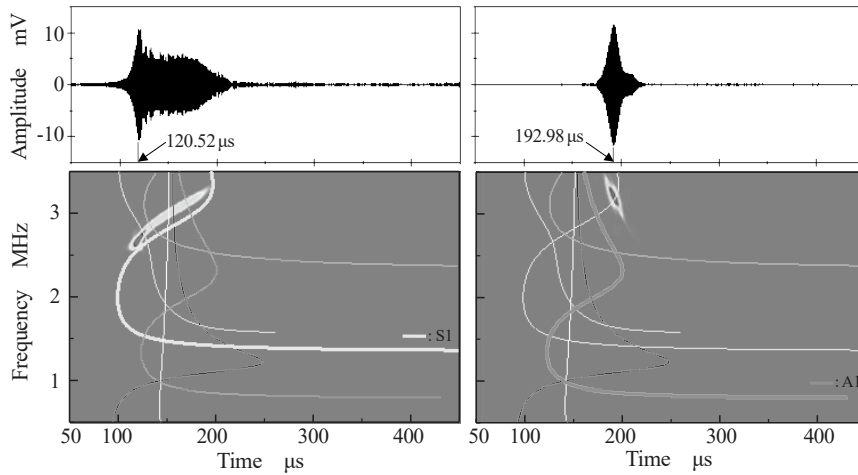


**Fig.6** Examples of the lamb waves detected from two kinds of specimens with the different slit shapes, their STFTs and group velocity dispersion curves for each mode. The frequency and the incidence angle for experimental conditions are 3.0 MHz and 34.4 deg, respectively. From these results, those waveforms were consisted of S1 and A1 mode, and it was able to find the cross points on the time-frequency plane obtained by MARS analysis.

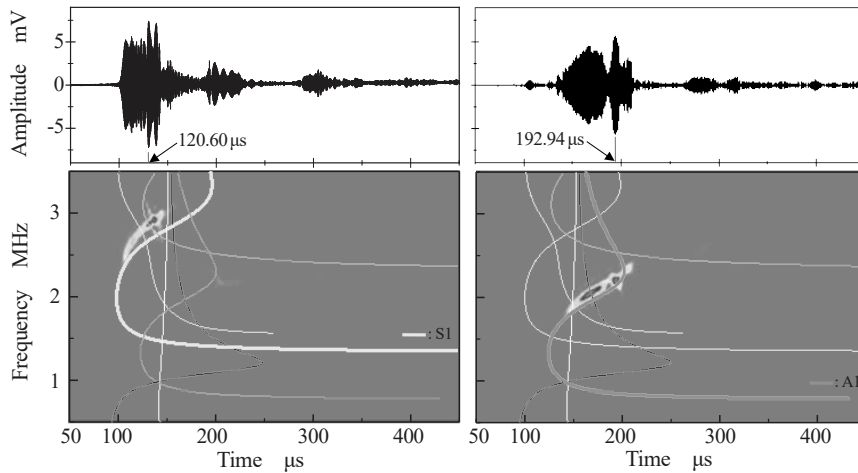
figure, the detected Lamb waves, the results of superimposing velocity dispersion curves on the STFT results of those waveforms, and the analysis results with the MARS method are shown, respectively. From the results in the center, it can be confirmed that both S1 and A1 modes exist in both waveforms. From the results in the bottom, it is evident that the frequency components of both modes of specimen type I and type II change with time, and the intersections of both lines indicating those changes were confirmed. The coordinates of the intersections were (190.00  $\mu$ s, 3.35 MHz) and (197.88  $\mu$ s, 2.281 MHz), respectively.

Figure 7 shows the results of the mode separation performed by the procedure described in Section 3.1 and the velocity dispersion curves superimposed on the STFT results. From the results in that figure, it is evident that each mode of S1 and A1 is separated. As a result of attempting to evaluate the thinning state by comparing the modes obtained from groove specimens with those obtained from the specimen with a uniform thickness of 2 mm, the following was clarified. The arrival time difference  $\Delta T_{ij}$  was calculated by the data of S1 mode waves (i.e., top left in Fig. 5(e) and Fig. 7(a) (b)) and A1 mode waves (i.e., top right in Fig. 5(e) and Fig. 7(a) (b)). As a result,  $\Delta T_{ij}$  of the specimens type I and type II were S1 mode: 0.80  $\mu$ s, A1 mode: -0.28  $\mu$ s and S1 mode: 0.88  $\mu$ s and A1 mode: -0.32  $\mu$ s, respectively.

Figure 8 shows the relationship between the groove depth  $d_i$  and the width  $w_j$  of each specimen by substituting each  $\Delta T_{ij}$  into Eq. (3). Here, the lines in blue and red denote the



(a) Results of mode separation of the lamb wave detected from specimen type I (depth: 0.4 mm, width: 5.0 mm)



(b) Results of mode separation of the lamb wave detected from specimen type II (depth: 1.0 mm, width: 2.0 mm)

**Fig.7** Examples of the lamb waves separated into each mode. Figure (a) and (b) show the lamb waves separated into each mode from the waves shown in Fig.6(a) (b). Also those STFTs and group velocity dispersion curves are shown. From these results, it was clarified that MARS method is able to be used to separate the two modes. Also, it is able to be seen that the left is for S1 mode and the right is for A1 mode.

results of S1 and A1 mode, respectively. Because each mode propagates the same thinning part, the state derived from each mode is the same. Therefore, the intersection of the lines of each mode showing the relationship between the groove depth  $d_i$  and the width  $w_j$  is the solution of the thinning state. Comparing the coordinates at the cross points with the measured values shows that they are almost the same under these experimental conditions, and it is demonstrated that the quantitative evaluation of the thinning state (depth and width of thinning part) is possible. The maximum errors of the depth  $d_i$  and width  $w_j$  with respect to the other grooved specimens prepared (see Fig. 1) in this study were  $\pm 0.082$  mm (10.25 %) and  $\pm 0.731$  mm (14.62 %), respectively. Considering the machining error, these results can be evaluated as appropriate estimations.

Since the above results were obtained, the specimens were prepared in which the groove shape of the above-mentioned specimen type I and type II was modified to the shape that

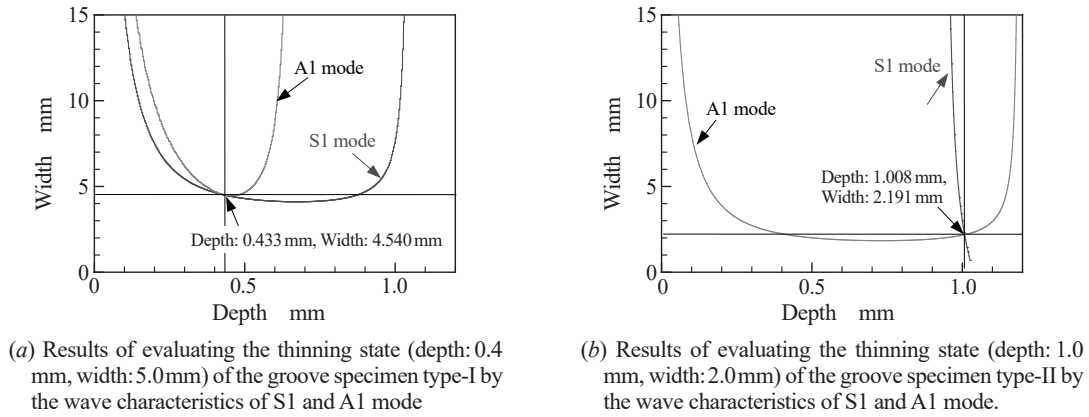


**Fig.8** Examples of evaluation results for the width and the depth of slit of each specimen. The relationships between the width and the depth are derived by using each data (*i.e.* S1 and A1 mode wave for each specimen shown in Fig.7) in Eq.(3) and are illustrated in this graph. The blue and the red color lines show the relationship between the depth and the width of the slit derived from each mode wave of S1 and A1. Here, the point where both lines intersect show the dimensions (*i.e.* depth and width) of the slit. It is evaluated that those results almost accord with the real dimensions of those slits.

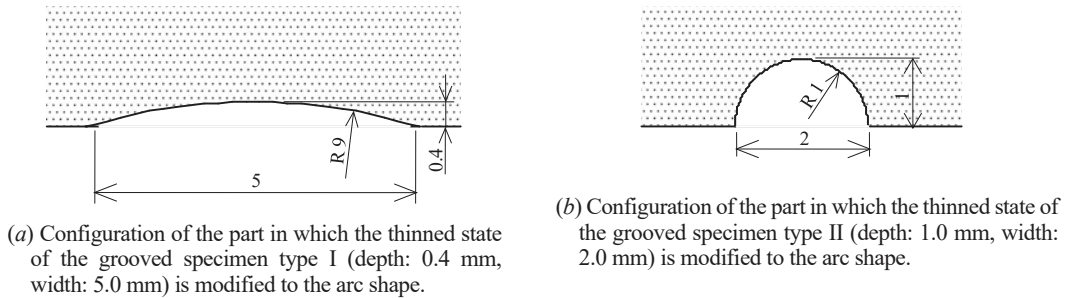


**Fig.9** The shapes and dimensions of the groove parts that were modified the groove shape of the specimen type-I and type-II to the shape that simulates the configuration that is considered to be caused by corrosion. The measured values for the depth  $d_i$  and width  $w_j$  of those shaped grooves were 0.318 mm (error: -20.50 %) and 3.702 mm (error: -25.96 %), 0.907 mm (error: -9.30 %) and 1.753 mm (error: -12.35 %) respectively. Those values became smaller than before modify, and the measurement accuracy decreased.

simulates the configuration considered to be caused by corrosion. Figure 9 shows the arc shape of the groove parts of these specimens. The measured values for the depth  $d_i$  and width  $w_j$  of the shaped grooves shown in Figs. (a) and (b) were 0.318 mm (error: -20.50 %) and 3.702 mm (error: -25.96%), 0.907 mm (error: -9.30%) and 1.753 mm (error: -12.35%), respectively. The values of both shapes became smaller than before modification, and the measurement accuracy decreased. This may be because the response of each Lamb wave mode at the frequency adopted to the shapes of which the wall thickness changes extremely slowly, as shown in Fig. (a). These results demonstrate that the origins of the errors include the lack of consideration for the mode conversion at the groove part and the adoption of low frequencies. The approach to deal with these issues will be considered in future research.

#### 4 Conclusion

In this study, a processing method for multiple-mode superimposed waves was proposed, so as to improve the defect detection resolution using Lamb waves with high-frequency components, and the effectiveness was examined. Specifically, the MARS method, which is a dynamic frequency analysis method, was applied to waves in which multiple modes are superimposed, and an evaluation of the wall thinning state based on the characteristics of the waveforms separated into each mode was attempted.

The MARS method was applied to each Lamb wave detected from the plate of uniform thickness and the grooved plate that simulated the wall thinning by corrosion, and each waveform was separated into each mode. Next, the method for evaluating the state (i.e., depth and width) of the groove from the difference in the arrival time of the same mode detected from the above mentioned two types of plates was proposed, and its effectiveness was demonstrated under the conditions of this experiment.

Future research will explore an evaluation method that considers the mode conversion in the wall thinning part and the improvement in evaluation accuracy.

#### Acknowledgment

We would like to express our gratitude to Mr. Jin Horiyama and Mr. Yuu Hinohara for their cooperation in carrying out this research while they were in graduate school at Kansai University.

#### References

- 1) Y. Mizutani, S. Inokawa, Y. Kurokawa and M. Mayuzumi. Nondestructive inspection of delamination in thin structures by using Lamb wave induced by chirp signal. *The Japanese Society for Experimental Mechanics*, 8 -1, 65-70 (2008) (in Japanese).
- 2) G. GuangJian, D. MingXi, L. MingLiang and P. JunFeng. Mode selection of Lamb waves for the evaluation of solid plates with liquid loading. *Science China Information Sciences*, 57 -10, 1840-1847 (2014).
- 3) H. Cho, T. Iegaki and T. Matsuo. Quantitative evaluation of wall thinning by corrosion using S0 mode Lamb waves. *Transactions of the Japan Society of Mechanical Engineers (Series A)*, 77 -779, 1056-1060 (2011) (in Japanese).
- 4) H. Cho, S. Koyama, T. Matsuo and M. Takemoto. Estimation of corrosion damage of plate structure using active Lamb waves, *Mechanical Engineering Congress Japan* (MECJ-06), Japan, 2006.
- 5) H. Cho, H. Nakazawa and M. Takemoto. Estimation method for wall reduction of plate-structure utilizing the fundamental Lamb waves, *Proc. Symp. Ultrason. Electron*, 24 P1-D-46, 97-98 (2003) (in Japanese).
- 6) M. A. Hamstad, A. O' Gallagher and J. Gary. A wavelet transform applied to acoustic emission signals -Part 1 Source identification-, *Journal of Acoustic Emission*, 20 , 39-61 (2002).

- 7) M. A. Hamstad, A. O' Gallagher and J. Gary. A wavelet transform applied to acoustic emission signals -Part 2 Source location-, *Journal of Acoustic Emission*, 20 , 62-82 (2002).
- 8) S. Minami and S. Kawata. "Introduction to data processing for scientific measurements," CQ Publishing Co., Ltd., 2002, pp.59-69 and pp.82-88 (in Japanese).